RSC Advances

PAPER

View Article Online
View Journal | View Issue

Cite this: *RSC Adv.*, 2021, **11**, 5149

First principle studies of ammonium chloride under high pressure

Mengya Lu,[a] Fubo Tian, *[a] Qiang Zhou[a] and Tian Cui *[ab]

Received 16th November 2020
Accepted 8th January 2021

DOI: 10.1039/d0ra09718g

rsc.li/rsc-advances

We performed a thorough high-pressure structural exploration of ammonium chloride up to 300 GPa by *ab initio* calculations. Two new phases, namely, $P2_1/m$ and *Cmma*, were predicted to be stable within the pressure ranges of 71–107 and 107–300 GPa, respectively. Like the known phase IV and V, the two new phases preserve alternate ammonium and chloride ions layer structures. The Bader charge analysis indicated that the numbers of electrons that N atoms get abruptly increased in the $P2_1/m$ phase. We also calculated the band gap and the variations in interatomic distances with pressure, and found the band gaps of two new phases decrease with increasing pressure and do not close up to 300 GPa.

Introduction

The high-pressure behavior of hydrogen-rich compounds is of great importance because of its role in high-temperature superconductors, such as H_3S,[1,2] CaH_6,[3] YH_{10},[4] and LaH_{10}.[5] The high superconducting transition temperatures (T_c) of H_3S (ref. 6) (200 K) and $LaH_{10\pm x}$ (ref. 7) (260 K) were confirmed experimentally. In this regard, scholars have focused on searching for other hydrogen-rich compounds. Ammonium halides, a vital family of hydrogen-rich compounds and potential candidate for high-temperature superconductors, have gained increasing attention because of their abundant transitions caused by relative orientations of ammonium ions.[8] Moreover, research on structure has been a hot topic because it is essentially related to superconducting properties.

Extensive theoretical and experimental efforts have been made to clarify the crystal structures of ammonium halides. The pressure–temperature phase diagrams of ammonium halides was determined at low pressure levels.[9–11] Thus far, NH_4Cl exists in four phases, namely, phase I (a disordered NaCl structure), phase II (a disordered CsCl structure), phase IV (an ordered CsCl structure), and phase V (a slightly distorted tetragonal CsCl structure). An ordered phase III only exists in NH_4Br[12,13] and NH_4I.[9,11,14] Moreover, we determined the structures of NH_4I and the related phase transitions at high pressure levels by using *ab initio* calculations,[15] and found that phase V is stable up to 74 GPa, at which ammonium iodine dissociates into NH_3, H_2, and I_2. Our group[12] also discovered that the phase V of NH_4Br transforms into monoclinic phase $P2_1/m$ at 71 GPa and to orthorhombic structure *Cmma* at 130 GPa. Although a large number of experiments for NH_4Cl were conducted, few studies have focused on its structure at high pressure levels.

In 1922, Simon[16] discovered the abnormal behavior of ammonium chloride, wherein it has a sharp transition in specific heat at −30 °C and ambient pressure. This phenomenon is called λ-type phase transition[17–20] or first-order transition. In addition, tricritical phase transition ($T_C = 257$ K) and second-order phase transition ($T_C = 267$ K) exist at 1.6 kbar (ref. 21–23) and 2.8 kbar, respectively.[24] We focused more on λ-type phase transition because it occurs not only in simple ammonium salts but also in some antiferromagnetic materials[25,26] and solid hydrogen.[27] Furthermore, many physical properties, such as coefficient of thermal expansion,[28,29] piezoelectric effect,[30,31] and dielectric constant,[32] vary sharply at the critical point. To investigate the nature of phase transition, scholars have made a great deal of effort experimentally[33–43] and theoretically.[44,45] The mechanism of order–disorder phase transition has been attributed to two possible orientations of ammonium tetrahedrons.[46]

At room temperature and low pressure, NH_4Cl adopts a CsCl-type structure (phase II), in which NH_4^+ ions are randomly distributed between two energetically equivalent orientations. When pressure is applied at room temperature, NH_4Cl transforms to phase IV,[42] which is referred to as ferro-ordered phase analogous to a ferro-magnet with parallel spin orientation of NH_4^+ between 9 and 10 kbar; this phase then transitions into phase V,[47] which has been proven in preliminary Raman measurements to exist in NH_4Cl at pressure levels higher than 110 kbar. To our knowledge, structures at high pressure or electronic properties have remained unexplored and are of great interest in research on NH_4Cl.

Computational methods

To search potential stable structures within the pressure range of 0–300 GPa, we used evolutionary algorithm methodology[48–53]

[a]State Key Laboratory of Superhard Materials, College of Physics, Jilin University, Changchun 130012, People's Republic of China. E-mail: tianfb@jlu.edu.cn
[b]Institute of High Pressure Physics, School of Physical Science and Technology, Ningbo University, Ningbo 315211, China. E-mail: cuitian@nbu.edu.cn

implemented in the USPEX code, which has been applied successfully to a wide range of crystalline systems. The simulation cell comprised of 1 to 4 formula units. The first generation consisting of 100 structures was generated randomly, and 60% of its low-energy structures were passed on to the next generation. The process was terminated after 40 generations. We then optimized the structures by using density-functional theory (DFT) with projector augmented wave (PAW) method[54] in the Vienna *ab initio* simulation package (VASP) code.[55] Local density approximation was used to describe the exchange–correlation function. To ensure that the total energy is well-converged to higher than 1 meV per atom, we chose a cut-off energy of 900 eV and Monkhorst–Pack *k*-points meshes[56] with a reciprocal space resolution of $2\pi \times 0.03$ Å^{-1}. Phonon dispersion calculations were performed with the PHONOPY code,[57] which is based on a supercell approach[58] with force constant matrices. The supercell consisting of 144 atoms of $2 \times 2 \times 3$ for $P4/nmm$ and *Cmma*, $3 \times 2 \times 2$ for $P2_1/m$ were used for the calculations.

Results and discussion

Fixed-composition structure prediction simulations were performed using the USPEX code considering unit cell sizes from 1 to 4 formula units for NH_4Cl up to 300 GPa. We discovered two novel structures with space groups $P2_1/m$ and *Cmma* for the first time. We calculated the enthalpy difference of phase V ($P4/nmm$) from 0 to 20 GPa with respect to phase IV ($P\bar{4}3m$) as a function of pressure (Fig. 1a). Fig. 1b shows the enthalpy difference of the two new phases relative to phase V within the pressure range of 60–300 GPa. Phase IV and V were repeatedly confirmed experimentally.[42,47,59,60] As shown in Fig. 1a, phase IV is stable thermodynamically below 12.9 GPa. Preliminary Raman measurements[47] indicated the transition pressure of phase IV to phase V (higher than 110 kbar), which is almost identical to our calculated results, thereby confirming the reliability of our calculation. In addition, phase V remains stable until 71 GPa, and new phase $P2_1/m$ emerges within 71–107 GPa. When the pressure reaches 107 GPa, the $P2_1/m$ phase transforms into the *Cmma* phase.

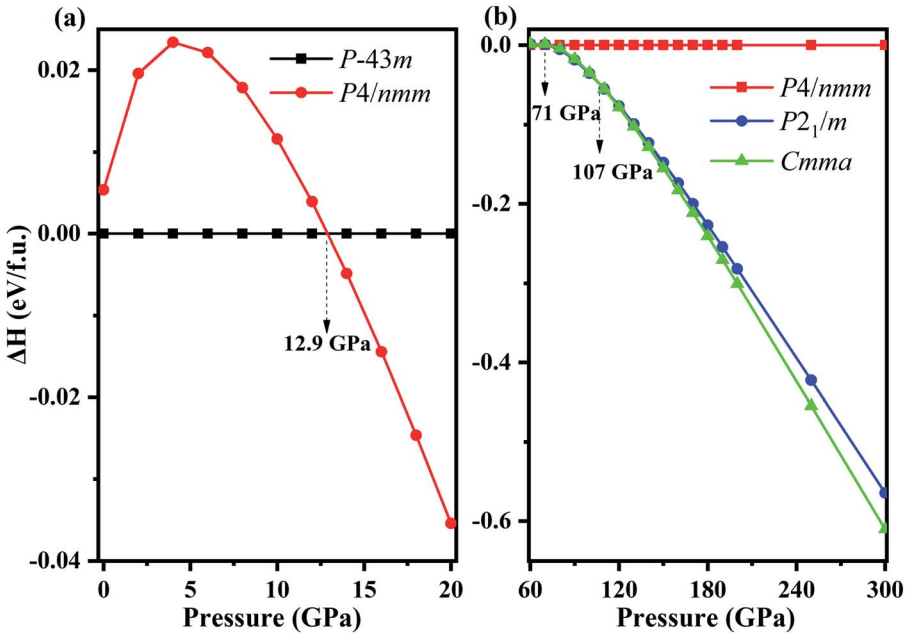

Fig. 1 (a) The enthalpy difference curves for phase V ($P4/nmm$) with respect to phase IV ($P\bar{4}3m$) as a function of pressure. (b) The enthalpy difference curves of predicted new phases with respect to phase V, the blue and green curves represent $P2_1/m$ phase and *Cmma* phase, respectively.

Table 1 Lattice parameters and atomic positions of new phases ($P2_1/m$ and *Cmma*)

Space group	Pressure/GPa	Lattice parameters	Atomic coordinates (fractional)
$P2_1/m$	80	$a = 2.8292$ Å, $b = 4.3915$ Å, $c = 4.4496$ Å, $\alpha = \gamma = 90°$, $\beta = 90.1756°$	H1 0.71576 0.44039 0.21126 H2 0.71855 0.75000 0.97815 H3 0.70044 0.75000 0.60091 N1 0.50244 0.25000 0.20585 Cl1 0.08653 0.75000 0.29497
Cmma	120	$a = 5.2907$ Å, $b = 7.0193$ Å, $c = 2.6471$ Å, $\alpha = \beta = \gamma = 90°$	H1 0.35533 0.58784 0.77272 N1 0.25000 0.50000 −0.00000 Cl1 0.00000 0.25000 0.39036

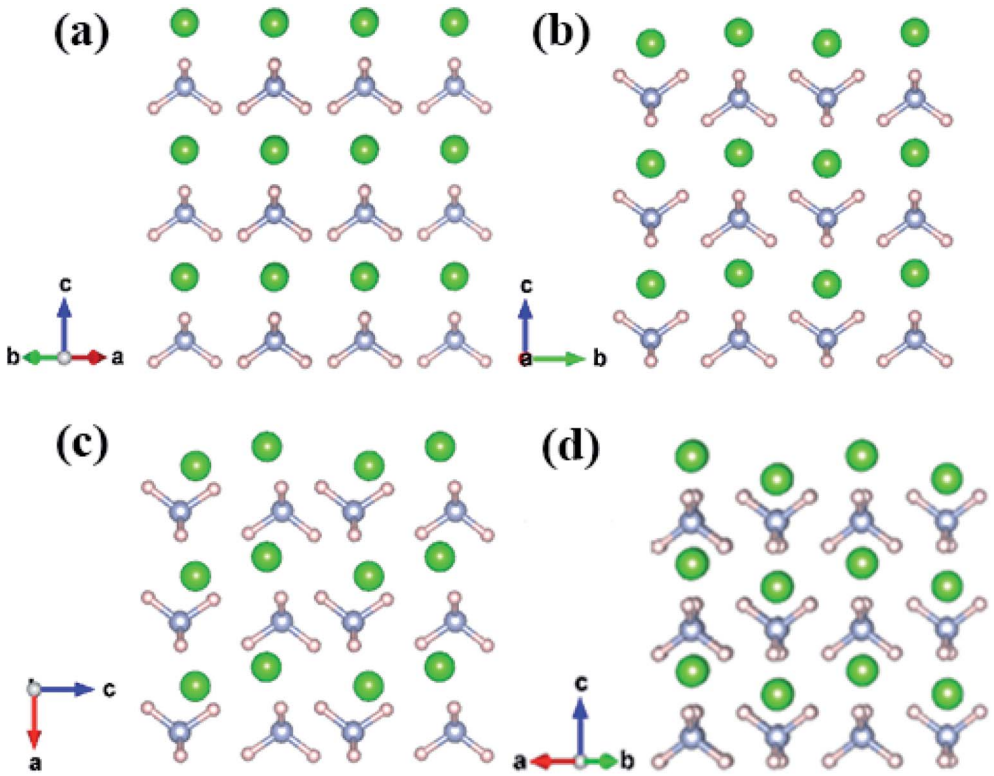

Fig. 2 The crystal structure of NH_4Cl for (a) phase IV, (b) phase V, (c) $P2_1/m$ phase and (d) *Cmma* phase. Green, pink and grey spheres represent Cl, H and N atom, respectively.

The lattice parameters and atomic positions of new phases are listed in Table 1. The *Cmma* remains stable up to 300 GPa.

Fig. 2 shows that all structures consist of well-separated ammonium and Cl ions. In particular, $P\bar{4}3m$ phase has a cubic structure, where eight ammonium ions are located in the vertices and chloride ions are situated in the body center. $P4/nmm$, $P2_1/m$, and *Cmma* structures have analogous configuration, where a chloride ion is surrounded by eight ammonium ions and each ammonium ion of the three phases forms a slightly distorted tetrahedron. In phase IV, ammonium ions have the same orientation (Fig. 2a). The four nearest N–H···I bonds are distributed on the diagonal lines due to fully ordered arrangement of ammonium ions in the $P\bar{4}3m$ structure. In $P4/nmm$ (b), $P2_1/m$ (c), and *Cmma* (d) structures, the orientation of ammonium ions on the diagonal lines remains consistent; as such, the four nearest N–H···I bonds are distributed on the same side. The antiparallel orientations lead to a dense structural packing, which is inevitable with enhanced pressure. This packing manner is also found in *Pnma* and *Cmcm* structures of CH_4.[61] Eventually, we found another intriguing phenomenon, that is, the four phases have layer structures, where Cl and ammonium ions are arranged alternately.

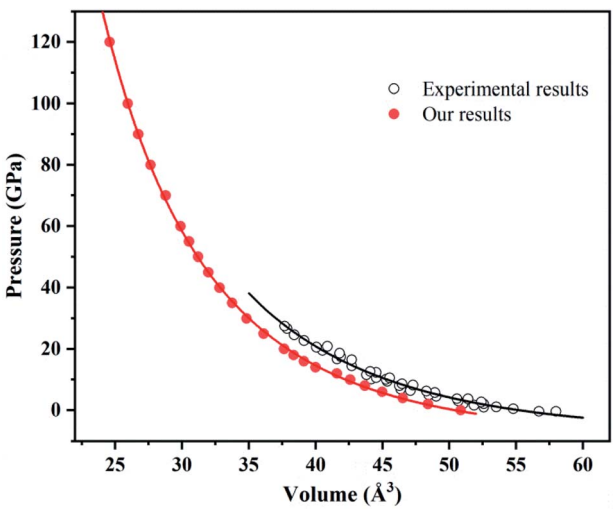

Fig. 3 Equation of states for ammonium chloride. Red solid circles and black open circles are from this work and experimental data,[62] respectively. Red solid line and black solid line illustrate the best fit of third-order BM EOS.

We also compared energy-dispersive X-ray diffraction data[62] at ambient temperature with the results at 0 K. We also determined the equation of state by fitting the pressure as a function of volume to the third-order Birch–Murnaghan EOS[63] as follows:

$$P = \frac{3B_0}{2}\left[\left(\frac{V_0}{V}\right)^{\frac{7}{3}} - \left(\frac{V_0}{V}\right)^{\frac{5}{3}}\right] \times \left[1 + \frac{3}{4}\left(B_0' - 4\right)\left(\left(\frac{V_0}{V}\right)^{\frac{2}{3}} - 1\right)\right] \quad (1)$$

The experimental data slightly differ from our calculated results within LDA possibly due to temperature. After all, temperature has great influence on volume (Fig. 3).

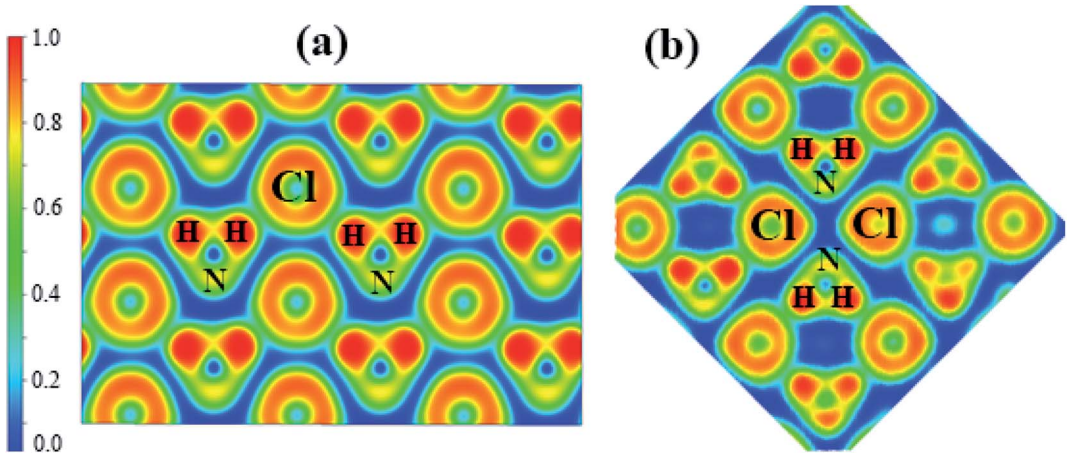

Fig. 4 The calculated electron localization function (ELF) maps of (a) phase $P2_1/m$ at 80 GPa, (b) phase *Cmma* at 120 GPa.

Table 2 The Bader charge analysis for NH_4Cl at different pressures

$P\bar{4}3m$ (6 GPa)	H1	H2	H3	H4	N1	Cl1
Charge	0.5215	0.5215	0.5215	0.5215	6.2259	7.6881
$P4/nmm$ (20 GPa)	H1	H2	H3	H4	H5	H6
Charge	0.5290	0.5290	0.5290	0.5290	0.5290	0.5290
	H7	H8	N1	N2	Cl1	Cl2
	0.5290	0.5290	6.2233	6.2233	7.6608	7.6608
$P2_1/m$ (80 GPa)	H1	H2	H3	H4	H5	H6
Charge	0.5418	0.5418	0.5418	0.5418	0.5461	0.5461
	H7	H8	N1	N2	Cl1	Cl2
	0.5337	0.5337	6.2409	6.2409	7.5955	7.5955
Cmma (120 GPa)	H1	H2	H3	H4	H5	H6
Charge	0.5457	0.5457	0.5457	0.5457	0.5457	0.5457
	H7	H8	H9	H10	H11	H12
	0.5457	0.5457	0.5457	0.5457	0.5457	0.5457
	H13	H14	H15	H16	N1	N2
	0.5457	0.5457	0.5457	0.5457	6.2374	6.2374
	N3	N4	Cl1	Cl2	Cl3	Cl4
	6.2374	6.2374	7.5797	7.5797	7.5797	7.5797

To understand the bonding nature, we calculated the electron localization function of the $P2_1/m$ phase at 80 GPa (Fig. 4a) and the *Cmma* phase at 120 GPa (Fig. 4b). We adopted Bader charge analysis to help elucidate the bonding nature. High ELF values indicate covalent bonds (>0.75), and values around 0.5 indicate uniform electron gas. We also calculated the ELF of phases IV and V, which are nearly identical to that of $P2_1/m$. Fig. 4a shows that Cl^- and NH_4^+ form zigzag chains. The highest ELF values are found between the N and H atoms of NH_4^+, indicating a strong covalent feature, which remains unchanged up to the highest pressure applied. Nevertheless, we found that only H atoms lose electrons, which are obtained by N and Cl atoms. As shown in Table 2, the numbers of electrons that H atoms transferred and Cl atoms obtained decrease with enhanced pressure. The numbers of electrons that N atoms obtained increase with pressure in general.

To verify the dynamic stability of several phases, we present the phonon dispersion curves of NH_4Cl along high-symmetry

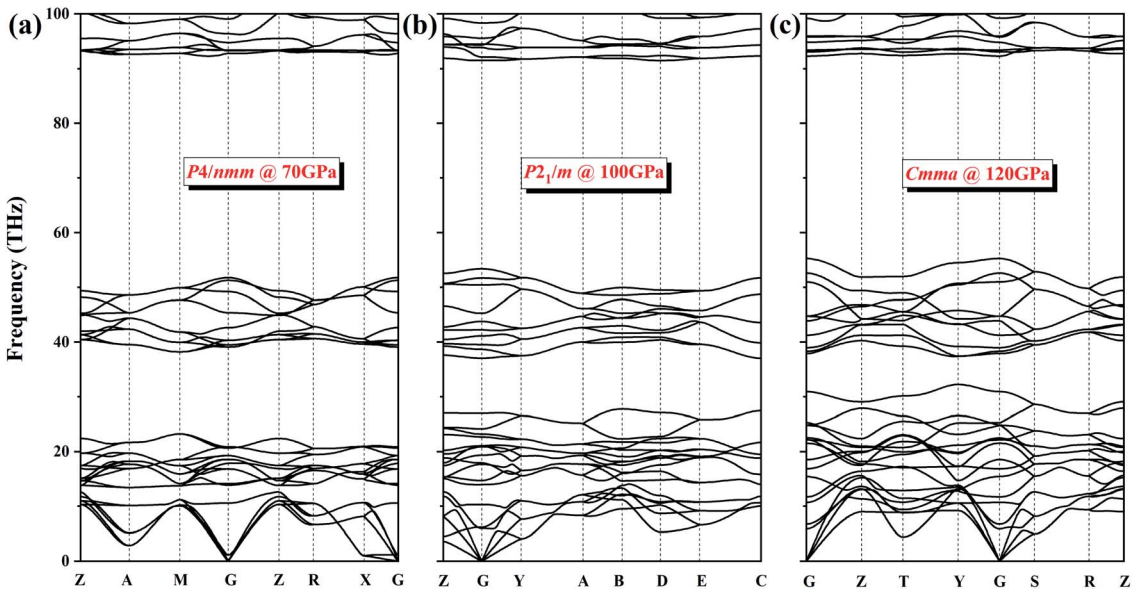

Fig. 5 The phonon dispersion curves of NH_4Cl for (a) $P4/nmm$ phase at 70 GPa, (b) $P2_1/m$ phase at 100 GPa and (c) *Cmma* phase at 120 GPa.

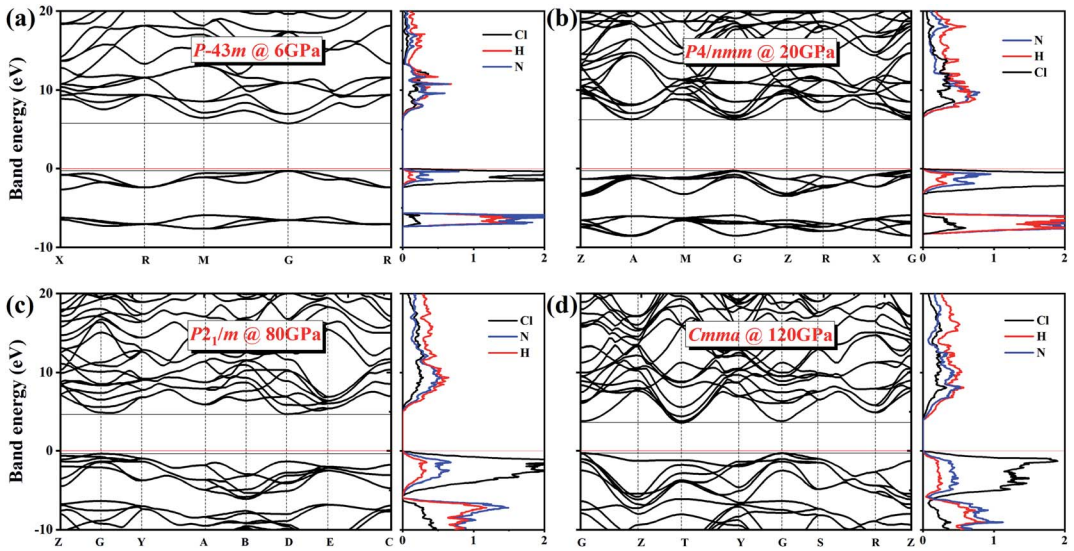

Fig. 6 Electronic band structures and density of states for (a) $P\bar{4}3m$ phase at 6 GPa, (b) $P4/nmm$ phase at 20 GPa, (c) $P2_1/m$ phase at 80 GPa, and (d) *Cmma* phase at 120 GPa. The red solid lines indicate the Fermi level.

directions for the $P4/nmm$ phase at 70 GPa, the $P2_1/m$ phase at 100 GPa, and the *Cmma* phase at 120 GPa (Fig. 5). In the three diagrams, no imaginary frequency is observed in the whole Brillouin zone. We can conclude that phase V ($P4/nmm$) is stable up to 71 GPa. Moreover, no imaginary frequency appears in the phonon spectrum of the two new phases. Thus, the $P2_1/m$ phase and the *Cmma* phase remain stable within 71–107 and up to 300 GPa, respectively.

We also explored the electronic band structures of the four stable structures at selected pressure levels (Fig. 6). Broad band gaps exist in the four phases. The density of states of conduction bands are mainly associated with H atoms. Below the Fermi, the bands can be separated into two parts: from the contribution of Cl atoms and from that of N atoms. With increasing pressure, the band dispersion becomes stronger below the Fermi level because of the decrease in the distance between N and Cl atoms. The plot of changes in band gap *versus* pressure is shown in Fig. 7. The band gap value increases first and then decreases when the $P\bar{4}3m$ phase transforms into the $P4/nmm$ phase, which is identical to that found in NH_4I.[15] In the pressure range of phase IV, the band gap increases with increasing pressure, which also occurs in most metallic oxides,[64,65] some zinc-blended semiconductors,[66,67] and metal hydrides.[68] Meanwhile, the band gap values of phase V and two new phases decrease with pressure, the situation is similar to most hydrides.[69–72]

We also studied the variations in interatomic distance with increasing pressure. We determined changes in the distance between N and H atom in NH_4^+ and between N and Cl atom in N–H···Cl (Fig. 8). The distance between N and H atoms decreases with increasing pressure, presenting a discontinuous

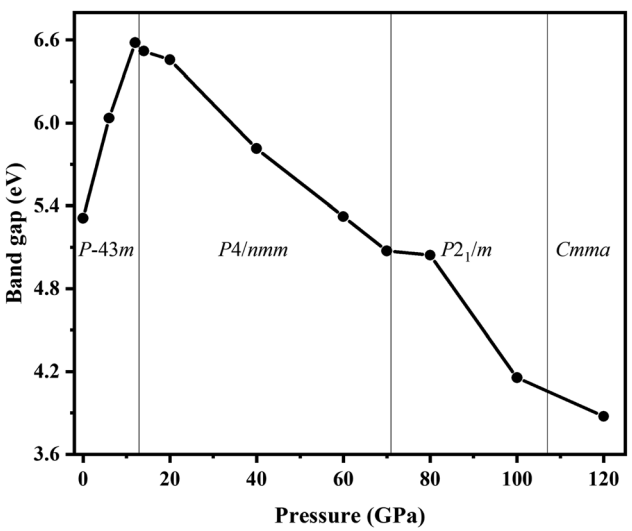

Fig. 7 The band gap *vs.* pressure for NH_4Cl up to 120 GPa.

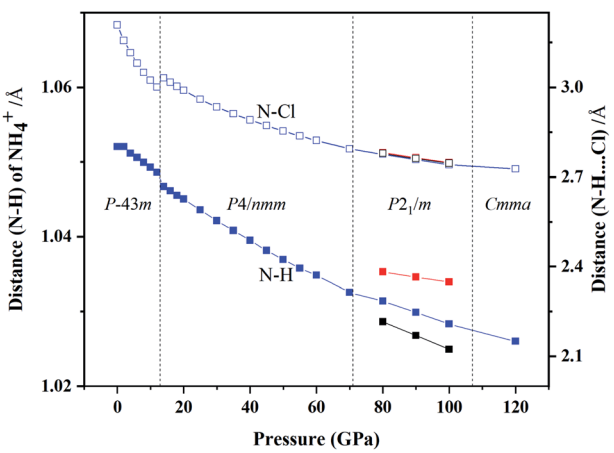

Fig. 8 The vary of interatomic distances with pressure. The left axis represents the distance between N and H atom in NH_4^+ (solid square), the right one represents the distance in N–H···Cl (hollow square).

jump at the transition point of phase IV into phase V and three different bond lengths of N–H exist in the $P2_1/m$ phase. The bond length of N–Cl increases abruptly at the phase transition pressure and then decrease with continuous increase in pressure.

Conclusions

In summary, the crystal structures, stability, and electronic properties of NH_4Cl at high pressure levels were investigated by *ab initio* calculations. We uncovered two new phases at high pressure, which are exactly the same as that of NH_4Br. The $P2_1/m$ phase exists within 71–107 GPa, and the *Cmma* phase is stable above 107 GPa up to at least 300 GPa. We also verified that the mechanism of IV–V phase transition is the 90° rotation of the NH_4^+ ions around the *c*-axis. In addition, the two new phases contain alternating layers of Cl and ammonium ions. NH_4Cl has not been metallized within the studied pressure range.

Conflicts of interest

There are no conflicts to declare.

Acknowledgements

This work was supported by the National Natural Science Foundation of China (No. 11574109, 51632002, 51572108, 91745203, 11574112), National Key Research and Development Program of China (No. 2016YFB0201204 and 2018YFA0305900). Program for Changjiang Scholars and Innovative Research Team in University (No. IRT_15R23), National Found for Fostering Talents of Basic Science (No. J1103202), Parts of calculations were performed in the High Performance Computing Center (HPCC) of Jilin University.

References

1 D. Duan, X. Huang, F. Tian, D. Li, H. Yu, Y. Liu, Y. Ma, B. Liu and T. Cui, *Phys. Rev. B*, 2015, **91**, 180502.
2 Y. Li, J. Hao, H. Liu, Y. Li and Y. Ma, *J. Chem. Phys.*, 2014, **140**, 174712.
3 H. Wang, S. T. John, K. Tanaka, T. Iitaka and Y. Ma, *Proc. Natl. Acad. Sci. U. S. A.*, 2012, **109**, 6463–6466.
4 F. Peng, Y. Sun, C. J. Pickard, R. J. Needs, Q. Wu and Y. Ma, *Phys. Rev. Lett.*, 2017, **119**, 107001.
5 H. Liu, I. I. Naumov, R. Hoffmann, N. Ashcroft and R. J. Hemley, *Proc. Natl. Acad. Sci. U. S. A.*, 2017, **114**, 6990–6995.
6 A. Drozdov, M. Eremets, I. Troyan, V. Ksenofontov and S. I. Shylin, *Nature*, 2015, **525**, 73–76.
7 M. Somayazulu, M. Ahart, A. K. Mishra, Z. M. Geballe, M. Baldini, Y. Meng, V. V. Struzhkin and R. J. Hemley, *Phys. Rev. Lett.*, 2019, **122**, 027001.
8 C. W. Pistorius, *Prog. Solid State Chem.*, 1976, **11**, 1–151.
9 H. Hochheimer, E. Spanner and D. Strauch, *J. Chem. Phys.*, 1976, **64**, 1583–1585.
10 W. Press, J. Eckert, D. Cox, C. Rotter and W. Kamitakahara, *Phys. Rev. B*, 1976, **14**, 1983–1988.
11 P. Andersson and R. G. Ross, *J. Phys. C: Solid State Phys.*, 1987, **20**, 4737–4743.
12 F. Tian, D. Li, D. Duan, C. Chen, Z. He, X. Sha, Z. Zhao, B. Liu and T. Cui, *Chin. Sci. Bull.*, 2014, **59**, 5272–5277.
13 H. A. Levy and S. Peterson, *J. Am. Chem. Soc.*, 1953, **75**, 1536–1542.
14 Y. Huang, X. Huang, L. Wang, G. Wu, D. Duan, K. Bao, Q. Zhou, B. Liu and T. Cui, *RSC Adv.*, 2015, **5**, 40336–40340.
15 M. Lu, Y. Huang, F. Tian, D. Li, D. Duan, Q. Zhou and T. Cui, *Chin. Phys. B*, 2020, **29**, 053104.
16 F. Simon, *Ann. Phys.*, 1922, **68**, 241–280.
17 A. W. Lawson, *Phys. Rev.*, 1940, **57**, 417–426.
18 N. Trappeniers, *Ber. Bunsenges. Phys. Chem.*, 1966, **70**, 1080–1084.
19 C. W. Garland and B. B. Weiner, *Phys. Rev. B*, 1971, **3**, 1634–1637.
20 H. Yurtseven and W. Sherman, *Phase Transitions*, 1995, **54**, 1–13.
21 B. B. Weiner and C. W. Garland, *J. Chem. Phys.*, 1972, **56**, 155–165.
22 H. Yurtseven and M. Baş, *J. Mol. Struct.*, 2000, **525**, 87–96.
23 H. Yurtseven, Ö. Tari and M. Baş, *J. Mol. Struct.*, 2001, **598**, 109–116.
24 M. Bas and H. Yurtseven, *ARI*, 1998, **51**, 136–140.
25 W. Robinson and S. Friedberg, *Phys. Rev.*, 1960, **117**, 402–408.
26 G. S. Dixon and J. E. Rives, *Phys. Rev.*, 1969, **177**, 871–877.
27 R. Hill and B. Ricketson, *London, Edinburgh Dublin Philos. Mag. J. Sci.*, 1954, **45**, 277–282.
28 A. Smits and C. Mac Gillavry, *Z. Phys. Chem.*, 1933, **166**, 97–112.
29 R. G. Ross and P. Andersson, *J. Phys. C: Solid State Phys.*, 1987, **20**, 4745–4762.
30 S. Bahrs and J. Engl, *Z. Phys.*, 1937, **105**, 470–477.
31 E. Mohler and R. Pitka, *Solid State Commun.*, 1974, **14**, 791–794.
32 A. C. Menzies and H. R. Mills, *Proc. R. Soc. London, Ser. A*, 1935, **148**, 407–422.
33 Y. Ebisuzaki and M. Nicol, *Chem. Phys. Lett.*, 1969, **3**, 480–483.
34 C. H. Wang and R. B. Wright, *J. Chem. Phys.*, 1974, **60**, 849–854.
35 C. H. Wang and R. B. Wright, *J. Chem. Phys.*, 1972, **56**, 2124–2129.
36 M. L. Shand, H. D. Hochheimer and C. T. Walker, *Solid State Commun.*, 1976, **20**, 1043–1047.
37 R. S. Krishnan, *Proc. Ind. Acad. Sci.*, 1947, **A26,**, 432–449.
38 G. Goldschmidt and D. Hurst, *Phys. Rev.*, 1951, **83**, 88–94.
39 H. Yamashita, *J. Phys. Soc. Jpn.*, 1970, **29**, 1391.
40 A. Heyns, *J. Phys. Chem. Solids*, 1980, **41**, 769–776.
41 A. Balagurov, D. Kozlenko, B. Savenko, V. Glazkov, V. Somenkov and S. Hull, *Phys. B*, 1999, **265**, 92–96.
42 A. Balagurov, B. Savenko, A. Borman, V. Glazkov, I. Goncharenko, V. Somenkov and G. Syrykh, *Inter. J. High Press. Res.*, 1995, **14**, 55–60.

43 V. Glazkov, D. Kozlenko, B. Savenko, V. Somenkov, G. Syrykh and A. Telepnev, *J. Exp. Theor. Phys.*, 2002, **94**, 1134–1139.
44 V. G. Vaks and V. Schneider, *Phys. Status Solidi A*, 1976, **35**, 61–72.
45 S. Salihoğlu, H. Yurtseven and H. KaraÇali, *Mol. Phys.*, 2007, **87**, 2371–2387.
46 H. A. Levy and S. Peterson, *Phys. Rev.*, 1952, **86**, 766–770.
47 S. J. Jeon, R. F. Porter and A. L. Ruoff, *J. Raman Spectrosc.*, 1988, **19**, 179–182.
48 A. R. Oganov and C. W. Glass, *J. Chem. Phys.*, 2006, **124**, 244704.
49 C. W. Glass, A. R. Oganov and N. Hansen, *Comput. Phys. Commun.*, 2006, **175**, 713–720.
50 A. R. Oganov, C. W. Glass and S. Ono, *Earth Planet. Sci. Lett.*, 2006, **241**, 95–103.
51 A. O. Lyakhov, A. R. Oganov and M. Valle, *Comput. Phys. Commun.*, 2010, **181**, 1623–1632.
52 A. R. Oganov, A. O. Lyakhov and M. Valle, *Acc. Chem. Res.*, 2011, **44**, 227–237.
53 A. O. Lyakhov, A. R. Oganov, H. T. Stokes and Q. Zhu, *Comput. Phys. Commun.*, 2013, **184**, 1172–1182.
54 G. Kresse and D. Joubert, *Phys. Rev. B*, 1999, **59**, 1758–1775.
55 G. Kresse and J. Furthmüller, *Phys. Rev. B*, 1996, **54**, 11169.
56 H. J. Monkhorst and J. D. Pack, *Phys. Rev. B*, 1976, **13**, 5188–5192.
57 A. Togo, F. Oba and I. Tanaka, *Phys. Rev. B*, 2008, **78**, 134106.
58 K. Parlinski, Z. Li and Y. Kawazoe, *Phys. Rev. Lett.*, 1997, **78**, 4063–4066.
59 Y. Ebisuzaki, *J. Chem. Phys.*, 1974, **61**, 3170–3180.
60 G. Venkataraman, K. U. Deniz, P. Iyengar, A. Roy and P. Vijayaraghavan, *J. Phys. Chem. Solids*, 1966, **27**, 1103–1123.
61 G. Gao, A. R. Oganov, Y. Ma, H. Wang and G. Zou, *J. Chem. Phys.*, 2010, **133**, 144508.
62 O. Schulte and W. Holzapfel, *High. Pres Sci. Technol.*, 1990, **4**, 321–323.
63 F. Birch, *J. Geophys. Res.: Solid Earth*, 1978, **83**, 1257–1268.
64 S. A. Gramsch, R. E. Cohen and S. Y. Savrasov, *Am. Mineral.*, 2003, **88**, 257–261.
65 Y. Wang, F. Tian, D. Li, D. Duan, H. Xie, B. Liu, Q. Zhou and T. Cui, *J. Alloys Compd.*, 2019, **788**, 905–911.
66 S. H. Wei and A. Zunger, *Phys. Rev. B*, 1999, **60**, 5404–5411.
67 O. Arbouche, B. Belgoumène, B. Soudini and M. Driz, *Comput. Mater. Sci.*, 2009, **47**, 432–438.
68 S. Zhang, J. Lin, Y. Wang, G. Yang, A. Bergara and Y. Ma, *J. Phys. Chem. C*, 2018, **122**, 12022–12028.
69 Y. Wang, R. Ahuja and B. Johansson, *Phys. Status Solidi B*, 2003, **235**, 470–473.
70 D. Meng, M. Sakata, K. Shimizu, Y. Iijima, H. Saitoh, T. Sato, S. Takagi and S.-i. Orimo, *Phys. Rev. B*, 2019, **99**, 024508.
71 D. Duan, Y. Liu, F. Tian, D. Li, X. Huang, Z. Zhao, H. Yu, B. Liu, W. Tian and T. Cui, *Sci. Rep.*, 2014, **4**, 6968.
72 L. Hao, Z. Yuan, X. Guo, Y. Zhang, K. Luo, Y. Gao, F. Ling, X. Chen, Z. Zhao and D. Yu, *Phys. Lett. A*, 2020, 126525.